Electroless deposition of nickel on biocompatible poly(dimethylsiloxane) after a laser processing as a pretreatment

Stephan Armyanov[1]*, Eugenia Valova[1], Konstantin Kolev[1], Dragomir Tatchev[1], Petar Atanasov[2], Nadya Stankova[2]

[1]*Institute of Physical Chemistry, Bulgarian Academy of Sciences, Sofia 1113, Bulgaria*
[2]*Institute of Electronics, Bulgarian Academy of Sciences, Sofia 1784, Bulgaria*

*Corresponding author

Abstract

Due to its biocompatibility poly(dimethylsiloxane) (PDMS) is an important material for the development of microelectromechanical systems or long-term, medical implants. The paper describes the morphology modifications and surface chemistry of PDMS during pulse laser treatment. SEM, μ-Raman spectroscopy, X-ray micro-tomography and XPS analyses are applied. PDMS decomposition takes place as a function of laser energy absorption. This leads to different oxidation degree of silicon, as shown by the curve fitting of Si 2p and O 1s. The irradiated parts become hydrophilic in contrast with the rest of the material, which remains hydrophobic. This is the condition enabling successful selective electroless deposition of Ni in the tracks, excluding the usual preceding sensibilization and chemical activation. This process is accomplished successfully after femtosecond laser irradiation and it is found that the time interval between laser treatment and metallization is not a critical parameter. Copyright © 2018 VBRI Press

Keywords: Electroless nickel, poly(dimethylsiloxane) PDMS, laser treatment, XPS, Raman spectroscopy, FE SEM, X-ray micro-tomography

Introduction

The wide-range-usage of poly(dimethylsiloxane) (PDMS) $((C_2H_6OSi)_n)$ is attributable to its physical and chemical properties: biocompatibility, oxidative stability, strength, durability, flexibility, gas permeability, easy moldability and transparency. Another advantage of using PDMS in electronic industries is its low-cost process compatibility [1]. Due to its properties, PDMS is an important material for the development of microelectromechanical systems or long-term, medical implants.

The possibility to metallize it is further expanding its application area. Different approaches are tried to realize this option. For example, recently, self-assembled monolayers of n-(2-aminoethyl) 3-aminopropyl-trimethoxysilane was used to improve the metal thin film adhesion, plated electrolessly onto PDMS [2].

The detail analysis of all methods, enabling the metallization of PDMS is beyond the scope of this paper. However, a very attractive one is the direct metallization by electroless deposition, possible after laser treatment. The electroless deposition of platinum immediately after PDMS treatment by excimer laser was demonstrated by Laude and his co-authors [3-7] and later in [8]. On this base was prepared a flexible electrode array [9]. However, the physicochemical side of the processes remains not clear enough.

In our previous papers, nanosecond (ns) and femtosecond (fs) laser processing of PDMS elastomer was discussed [10-13]. As a result of the preliminary investigations hydrazine was selected as a reducer for electroless plating of nickel [12, 13]. It produces practically pure nickel coatings, excluding incorporation of phosphorus or boron, when hypophosphite or dimethylamine-borane is applied. There are also other attractive features of this type of coatings for the electronic industry.

The aim of this paper is to present a summary of the physical and chemical transformations of the PDMS after the formation of ablation tracks, making possible the filling of these tracks with metal by electroless plating: nickel for the beginning and platinum to be the next. To our data published before the results of new investigations are added outlining better and more completely the physicochemical matter of the observed phenomena.

Experimental

Material and treatment details

PDMS-elastomer sheets (KCC-corporation, South Korea) (800 μm thick) are irradiated with basic harmonic (λ = 1064 nm), as well as second harmonic generation (SHG) (λ = 532 nm), third harmonic generation (THG)

(λ = 355 nm) and fourth harmonic generation (FHG) wavelength (λ = 266 nm) of Q-switched Nd:YAG ns laser (pulse duration τ = 15 ns and pulse repetition rate of 10 Hz). The laser beam is focused by a lens with 22 cm focal length.

The material is also processed by chirped-pulse-amplification fs laser Nd: glass laser system providing pulses at the fundamental wavelength of λ = 1055 nm, SHG (λ = 527 nm) and FHG (λ = 263 nm) (pulse duration $\tau \approx$ 300 fs and repetition rate of 33 Hz). The laser beam is focused perpendicularly to the sample surface using lenses with 7.5 cm focal distance.

The laser processing is performed in air at ambient temperature in a multiple pulsed regime in order to obtain continuous tracks. The line tracks are obtained by overlap (up to 90%) of the adjacent laser beam spots. The samples are mounted on a moving stepper-motor computer-controlled X–Y table. The micro-channels (tracks) are produced in ''scanning mode'' by simultaneously moving the samples perpendicularly to the laser beam with a speed in the interval of 8–76 μm/s in the case of ns laser. The number of the consecutive pulses (from 8 to 110) per laser beam spot on the material surface is controlled by the moving speed of the table. Continuous tracks with lengths between 3 and 10 mm and widths between 50 and 500 μm, depending on the laser parameters, are produced. Larger widths are made especially for the samples prepared for XPS analyses.

In case of fs laser two scanning speeds of 38 μm/s and 95 μm/s, corresponding to 83 and 33 overlapping pulses are applied.

Before laser treatment, the PDMS samples are cleaned by the following steps: cleaning in a detergent solution using ultrasonic bath (USB); rinsing with deionized water; cleaning again with ethanol in USB; and finally filtered air stream drying. After laser treatment, PDMS samples were prepared for metallization as follows. First, they were cleaned in a detergent solution, using USB for 10 min. Then they were thoroughly washed with deionized (DI) water. Followed sonication with ethanol and drying with air stream. Cleaning is an important step to avoid quick spontaneous decomposition of electroless solutions.

As a result of comparative investigations, after the laser treatment the most suitable bath for electroless deposition onto PDMS using hydrazine hydrate turned to be this, proposed by H. Honma and collaborators [**14**]. The composition of the solution [M] and plating conditions are as follows: $NiCl_2 \cdot 6H_2O$ 0.05, $H_2NNH_2 \cdot H_2O$ 0.4, H_3BO_3 0.5, NH_2CH_2COOH 0.3, pH12, T = 85-90°C.

In the preliminary experiments 20×10 mm substrates of copper foil, 70 μm thick, were used. They were cleaned with degreaser, thoroughly rinsed with tap and DI water stream, and consecutively washed in USB with ethyl alcohol and acetone. Then after cleaning in $K_2S_2O_8$ aqueous solution 5 g/l for 2 min, immersion treatment followed in a 10 g/l of H_2SO_4 for 1 min. After each procedure, the Cu substrates were rinsed thoroughly with DI water. Finally, activation was carried out for 3 min in a solution containing: $PdCl_2$ (anhydrous, 59.87%, Aldrich) 0.001 M, HCl (37%) 0.1 M. The plating was conducted in

a thermostated vessel, under rigorous stirring. On the copper substrate, nickel was electroless deposited in the main solution.

In contrast, onto laser treated PDMS the deposition was performed without sensibilization and activation. After metallization, the samples were washed with DI water and dried.

Measurements

Different experimental techniques were applied to characterize the pristine PDMS-elastomer, as well as the irradiated tracks: ZEISS Ultra-55 field emission Scanning Electron Microscope (SEM); μ-Raman spectrometry (LabRAM HR Evolution-Horiba Scientific), equipped with 100× magnification objective and excited by solid state laser source operating at λ = 532 nm.

X-ray Photo electron Spectroscopy (XPS) studies were performed in a PHI model 5600 system equipped with an Omni Focus Lens III using a standard Mg Kα X-ray source at a high voltage of 15 kV, 300 W. The PHI Multipak 9 software was used for data treatment and interpretation.

Computerized tomography (CT) investigation was carried out with a Bruker SkyScan1272 X-ray microtomograph.

Results and discussion

A selection of the most substantial results representing the laser treatment effects and electroless deposition will be shown.
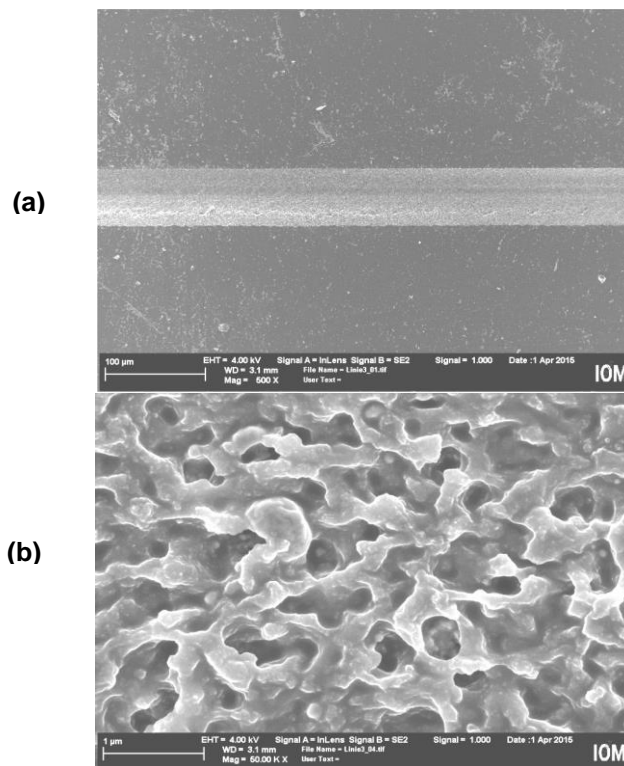

Fig. 1. FE SEM images of the track in PDMS, processed by fs laser, λ 263 nm, pulse duration 300 fs, 83 pulses, laser fluence 1.04 J/cm^2: **a**) low magnification, **b**) high magnification.

The appropriate laser processing parameters cause ablation and the typical picture of the formed tracks is exposed in **Fig. 1a**. It is clear that the profile of the tracks is characterized by extremely developed surface with caves, which could promote good adhesion of the metal coating deposited on it through the so called "anchoring" effect: **Fig. 1b**.

Fig. 2 displays the μ-Raman spectra of non-processed (pristine) and laser processed PDMS applying near-infrared (NIR) irradiation, typical for both ns and fs radiation [**10-13**]. As a result of laser treatment, one can see a sharp peak of crystalline silicon adjacent to the peaks of pristine PDMS. Its intensity increases with laser fluence and number of sequential laser pulses at all applied laser wavelengths. At higher fluence and number of pulses broad bands assigned to the D band of amorphous carbon and the G band of polycrystalline and microcrystalline graphite also appear, confirming findings described before [**10-12**, **15**, **16**].
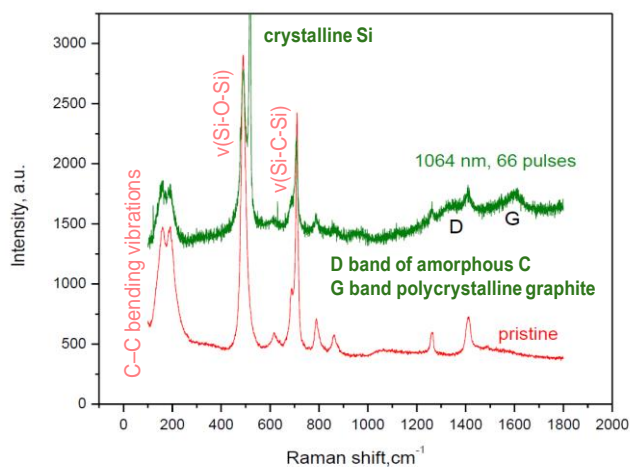

Fig. 2. μ-Raman spectra of pristine and treated by ns laser PDMS. Irradiation with λ 1064 nm, 66 pulses, fluence 6.4 J/cm^2.

The hypothetical picture of laser treatment effect should involve the possible scission of linkages in the molecular structure of PDMS. Based on the bond dissociation energies: 3.73 eV of Si-C; 4.28 eV of C-H and 4.68 eV of Si-O [**17**], this sequence of direct photochemical bond breaking can be realized. The condition for this is laser energy absorption exceeding those energies.

Thus, as a function of laser fluence and number of pulses, silicone elastomer decomposition takes place. This implies the evolution of the Si-O bond should be investigated in more details.

Whenever shifts in the positions of Si 2p and O 1s appear, their evaluation needs precise XPS calibration. A natural choice for this is carbon, since its peak is present on all samples exposed to the environment [**18**, **19**]. In this case, C 1s is adjusted at a binding energy (BE) of PDMS 284.38 eV [**20**, **21**].

It turns out that the Si 2p BE peak position of the sample, treated by ns laser NIR irradiation and 66 pulses, is shifted by 0.9 eV with respect to the pristine PDMS. This

can be caused by the introduction of oxygen, as it is shown to occur after plasma treatment in [**22**]. In addition, at the same sample BE of O 1s peak is shifted by 0.4 eV. This peak position reflects a stronger oxidation of Si. Further, the profile of O 1s and Si 2p peaks are analyzed in details.

The deconvolution of Si 2p peak after this particular laser treatment is displayed in **Fig. 3** and **Table 1** and it is clear, that oxidation to different degree takes place. It is claimed for pure silicon (Si) a peak at 99.5 eV corresponding to Si(–OH)$_x$ could exist [**26**]. In our case, it is hard to identify such a peak. It looks like the chemical condition of Si of PDMS is determined mainly by its position in the polymer chain and during the oxidation process by bonding with oxygen. In other words, one can expect very low influence of H through O on the BE of Si 2p in this case.
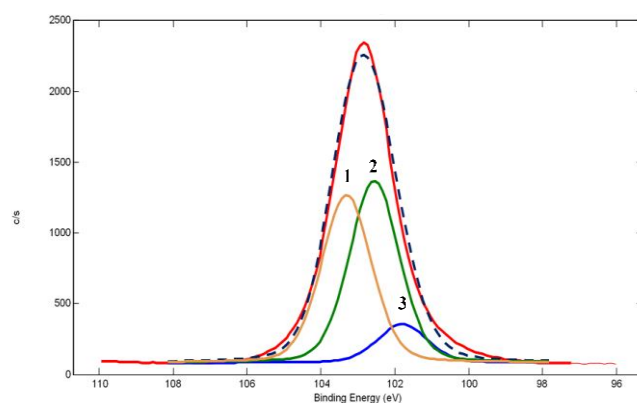

Fig. 3. Curve fitting of XPS spectra of Si 2p for treated by ns laser λ 1064 nm 66 pulses 6.5 J/cm^2. The red line displays original peak, the dashed line is the fitting curve. Orange line (1) Si(-O)$_4$ 103.3 eV, green line (2) Si(-O)$_3$ 102.6 eV, blue line (3) Si(-O)$_2$ 101.8 eV; The areas under the curves are as follows (**Table 1**): Si(-O)$_2$ 10.0%, Si(-O)$_3$ 46.8 %, Si(-O)$_4$ 43.2 % [**11**].

Table 1. Silicon chemical environments and the corresponding Si 2p (See also [**21**, **23**-**26**]).

Structure	O O–Si–O O	O O–Si–O CH$_3$	CH$_3$ O–Si–O CH$_3$
Abbreviation	Si(-O)$_4$	Si(-O)$_3$	Si(-O)$_2$
Experimental BE (eV)	103.3	102.6	101.8
Reference BE (eV)	103.3	102.67	101.79
Source	SiO$_2$ [**26**]	[**25**]	PDMS [**21**, **23**]
Calculated from fitting in **Fig. 3** (%)	43.2	46.8	10.0

Similar supposition was made for the absence of (–OH) related peaks in Fourier Transform Infrared Spectroscopy of treated PDMS [**27**]. Free SiOH could be quantitated eliminating the water and siloxane interferences in a siloxane band applying dissolution of PDMS in carbon tetrachloride [**28**].
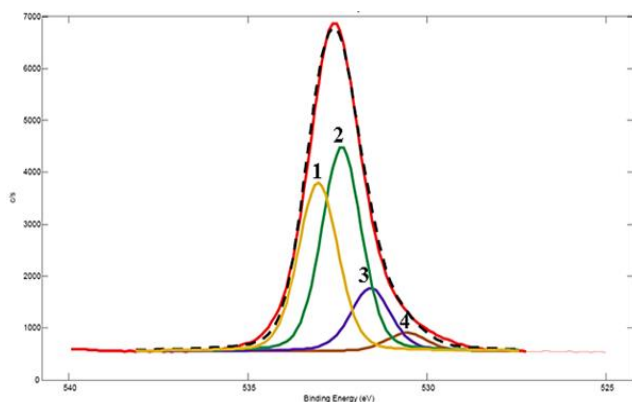
Fig. 4. Curve fitting of XPS spectra of O 1s for treated by ns laser λ 1064 nm 66 pulses 6.5 J/cm². The red line displays original peak, the dashed line is the fitting curve. The areas under the curves (**Table 2**): orange (1) Si(-O)$_4$)) 36.9 %, green (2) (Si(-O)$_3$) 44.6 %, , purple (3) (Si(-O)$_2$) 14.4%, dark orange (4) (Si(-OH)) 4% [**11**].

Table 2. Oxygen chemical environments and the corresponding O 1s BE.

| Structure	O | O–Si–O | O	O | O–Si–O | CH$_3$	CH$_3$ | O–Si–O | CH$_3$	OH | O–Si–O | CH$_3$
Abbreviation	Si(-O)$_4$	Si(-O)$_3$	Si(-O)$_2$	Si(-OH)
Experimental BE (eV)	533.0	532.4	531.6	530.6
Calculated from fitting in **Fig. 4** (%)	36.9	44.6	14.4	4.0

The curve fitting of O 1s peak is presented in **Fig. 4** and **Table 2**. For SiOH in as-received pure Si one could see BE of about 530.4 eV in Fig. 5 of [**22**]. In the case of special treatment of Si in condition of humidity the BE of Si(OH)$_x$ is about 1 eV higher. [[**22**], and references therein]. Also for other substances, different from PDMS, it is reported that BE of O 1s for SiO$_{1.8}$ is 532.20 eV [**29**], for SiO$_{1.9}$ is 532.6 eV [**30**], and for SiO$_2$ 533.20 eV [**31**]. Thus, it is expectable the peak shift to higher values of BE, when the oxidation degree of Si in PDMS is increased. However, it is hard to make exact predictions.

From the data shown in **Fig. 4** and **Table 2** one can see the BE values of the peaks after the deconvolution are close to the mentioned above for oxidation forms of the pure Si. The areas under the three peaks in **Fig. 3** and **Table 1** are of the same order as the respective three peaks in **Fig. 4** and **Table 2**.

The presence of OH groups on the surface is responsible for hydrophilic behavior of laser treated areas, being one of the factors enabling electroless metallization. However, the photochemical conversion of surface methylsilane groups (Si–CH$_3$) to silanol groups (Si-OH) on the PDMS surface is responsible for the large increase in surface free energy. Thus, after laser irradiation with time a subsequent degradation of the polymer and formation of SiO$_x$ was observed [**32**].

The detailed results of this degradation are described in **Figs. 3** and **4**. The decreasing of the number of silanol groups on the PDMS surface is the reason for continuously decreasing of hydrophilicity and its rejuvenation to enable the metallization by electroless plating is a challenging task. A possible recovering of the surface after the laser ablation during one month lapse between the laser treatment and XPS measurements cannot be excluded. Similar phenomena after plasma treatment of PDMS were observed [**33**].
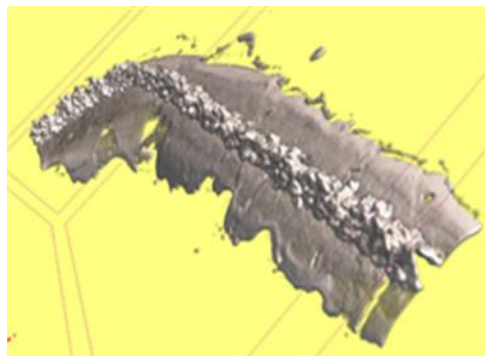
(a)
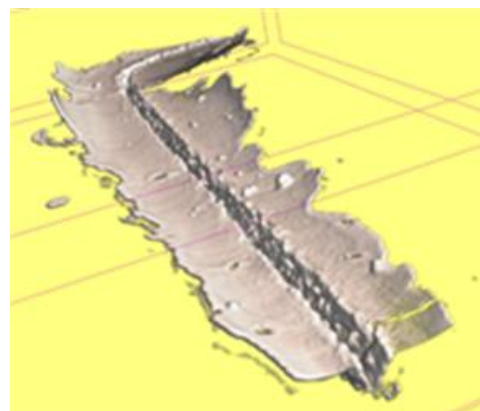
(b)

Fig. 5. X-ray micro-tomography images of a Ni-filled track on PDMS MED 4860. Top view (a) and view from the bottom (b).

The shape of nickel coating in the beginning of plating formed inside the track, created by laser, is demonstrated in **Fig. 5**. Due to the difference in density, PDMS is not seen and nickel coating is only revealed. **Fig. 5** illustrates the ablation profile formed by UV Nd:YAG ns pulsed laser. The radiation parameters are: λ = 355 nm, laser spot diameter 150 μm, laser energy 4.3-4.9 J/cm², pulse duration 15 ns and pulse frequency (repetition rate) 10 Hz.

Fig. 5 illustrates that due to ablation by ns laser, a part of the material is thrown aside. Similar to the track surface, it is activated for electroless plating. In the beginning of plating the coating is just decorating sensitive areas covering it uniformly. The bottom of the Ni plate shows the rough morphology of the track surface. Nickel coating outside the channel onto the thrown out from the track material is parasitic, with weak adhesion and subject to easy detachment.

Before to plate nickel in PDMS tracks the evolution of the nano morphology with its thickness on copper substrate is investigated in details. Initial and final stages are illustrated in **Fig. 6**. It is seen that in the beginning (**Fig. 6a**) the coating is covering uniformly the substrate (similar to what is shown in **Fig. 5**). Such a behavior is very beneficial. After 30 min of deposition a nano dendritic structure is developed. More about the factors enabling the formation the Ni nano-spikes can be found in [**34**, **35**].

(a)
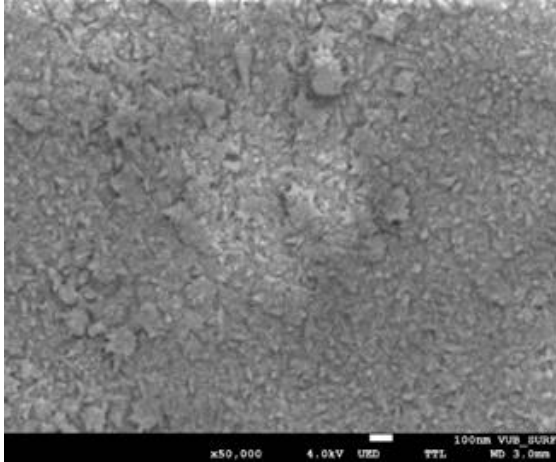
(b)
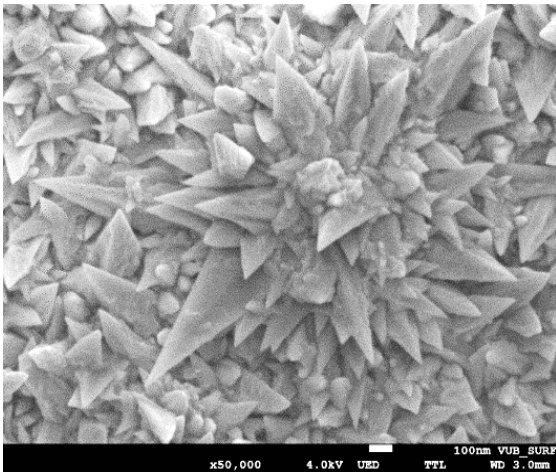
Fig. 6. Morphology of electroless Ni coatings on Cu substrate. Deposition time (min): a) 3, b) 30.

After filling up the track by nickel, the surface nano morphology is well seen in **Fig. 7**, similar to the demonstrated in **Fig. 6b**. The significance of this type of nano morphology is connected with the fact that the microscopic surface roughness of the metal plays a large part in determining the electrode impedance [**36**]. This is the reason in the tracks, formed due to the PDMS laser ablation, to plate nickel coatings with a final rough surface, as it is shown in **Fig. 7.** No additional operation is performed after the fs laser treatment. Moreover, it is important to mention that the metallization was not performed almost immediately after the tracks formation as it was made before using excimer laser [**3-9**].

It looks like the electroless deposition becomes possible after reaching a suitable balance between the photochemical and photothermal effects of the irradiation. This balance depends in descending order on the wave length, pulse duration, number of pulses and energy per pulse and fluence. At each wave length there is specificity [**13**]. However, the number of pulses 83 have decisive role for the deposition of Ni, when fs laser is used.

The obtained results will facilitate the electroless plating of pure platinum instead of nickel using hydrazine as a reducer. This will be a subject of the further investigations.
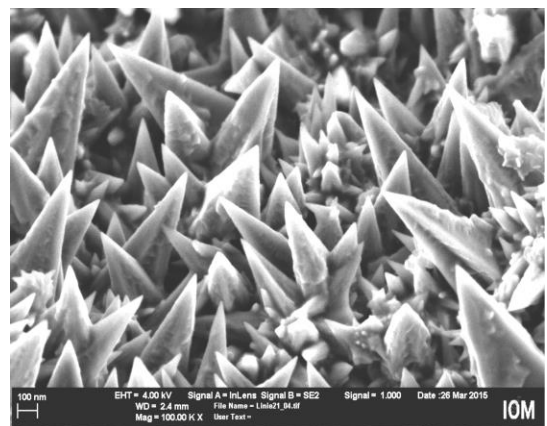
(a)
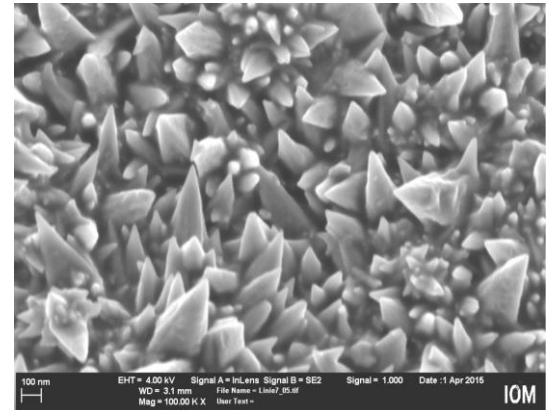
(b)
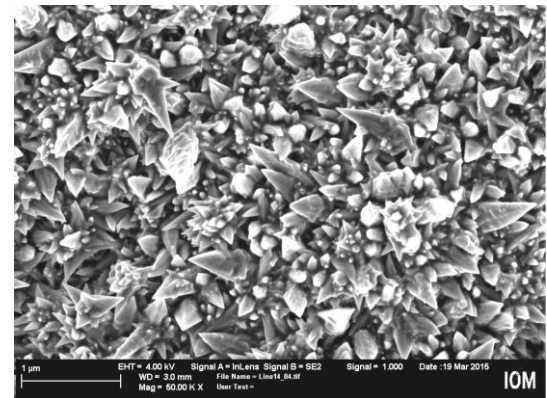
(c)

Fig. 7. SEM microphotographs of the electroless Ni metalized PDMS tracks, formed by fs-laser at: a) UV (λ 263 nm) laser pulses 300 fs at fluence 1.5 J/cm^2; b) VIS (λ 527 nm) laser pulses 300 fs at fluence 1.8 J/cm^2; c) NIR (λ 1055 nm) laser pulses 900 fs at fluence 2.7 J/cm^2. In all cases, the images refer to 83 overlapping pulses (scanning speed of 38 μm/s).

Conclusion

There are two key issues enabling metallization by electroless plating after the laser treatment: first, to form patterns, where hydrophobic surface of the pristine PDMS is converted into hydrophilic track and second, to produce well-developed surface roughness in it, enabling good adhesion. Electroless plating of nickel into fs-laser formed tracks in PDMS is performed using hydrazine as reducing agent without any additional pretreatment. The electroless deposition becomes possible in PDMS tracks after reaching a suitable balance between the photochemical and photothermal effects of the irradiation. It is found that, when femtosecond laser is applied, the time interval between laser treatment and metallization is not a critical process parameter, as it was considered before.

References

1. Qin, Y.; Howlader, M.M.R.; Deen, M.J.; Haddara, Y.M.; Selvaganapathy, P.R.; *Sens. Actuat. B: Chem.,* **2014**, *202*, 758-778. **DOI:** 10.1016/j.snb.2014.05.063
2. Molazemhosseini, A.; Ieffa, S.; Vena, P.; Magagnin, L.; *ECS Transact.*, *66*, **2015**, 13-22. **DOI:** 10.1149/06619.0013ecst
3. Laude, L.D.; European patent 0693138B1, 1997.
4. Laude, L.D.; U. S. patent US 5,599,592, 1997.
5. Laude, L.D; Kolev, K ; Dicara, C.; Dupas-Bruzek C.; Proc. SPIE; *Vol. 4977*, 578-586, **2003**. **DOI:** 10.1117/12.483853
6. Dicara, C.; Robert T. ; Kolev, K.; Dupas-Bruzek, C.; Laude, L.D.; ALT'02 International Conference on Advanced Laser Technologies, 255. (November 14, 2003) Proc. SPIE; *Vol.* 5147, 255-265, **2003**. **DOI:** 10.1117/12.537694
7. Laude, L.; Talbot, N.H.; Greenberg, R.J.; European patent EP 1971704 A2, WO 2007058975A2, 2008. 24 Sept.
8. Dupas-Bruzek, C.; Dréan, P.; Derozier, D.; *J. Appl. Phys.*, **2009 ;** *106*, 074913-1–074913-5, **DOI:** 10.1063/1.3236509
9. Laude, L.D.; Greenberg, R.J.; USP 7749608 B2 (2010).
10. Atanasov, P.A.; Nedyalkov, N.N.; Valova, E.I.; Georgieva, Z.S.; Armyanov, S.A.; Kolev, K.N.; Amoruso, S.; Wang, X.; Bruzzese, R.; Sawczak, M.; Sliwinski, G.; *J. Appl. Phys.* **2014**;*116*: 023104-1–023104-4. **DOI:** 10.1063/1.4887812
11. Armyanov, S.; Stankova, N.E.; Atanasov, P.A.; Valova, E.; Kolev, K.; Georgieva, J.; Steenhaut, O.; Baert, K.; Hubin, A.; *Nucl. Instr. Meth. Phys. Res. B*. **2015**, *360*, 30-35. **DOI:** 10.1016/j.nimb.2015.07.134
12. Stankova, N.E.; Atanasov, P.A.; Nedyalkov, N.N.; Stoyanchov, T.R.; Kolev, K.N.; Valova, E.I.; Georgieva, J.S.; Armyanov, S.A.; Amoruso, S.; Wang, X.; Bruzzese, R.; Grochowska, K.; Sliwinski, G.; Baert, K.; Hubin, A.; Delplancke, M.P.; Dille, J., *Appl. Surf. Sci*., **2015**, *336*, 321-328. **DOI:** 10.1016/j.apsusc.2014.12.121
13. Atanasov, P.A.; Stankova, N.E.; Nedyalkov, N.N.; Fukata, N.; Hirsch D.; Rauschenbach, B.; Amoruso, S.; Wang, X.; Kolev, K.N.; Valova, E.I.; Georgieva, J.S.; Armyanov, S.A., *Appl. Surf. Sci*., **2016**, *374*, 229–234. **DOI:** 10.1016/j.apsusc.2015.11.175
14. Tashiro, K.; Watanabe, T., Inaba, H.; Honma, H.; Electroless nickel plating using hydrazine reducing agent with excellent bath stability. *J. Surf. Finish. Soc. Japan*, **2000**, *51*, 606-611.
15. Graubner, V.-M.; Nuyken, O., Lippert, T.; Wokaun, A.; Lazare, S.; Servant, L.; *Appl. Surf. Sci.*, **2006**, *252*, 4781-4785. **DOI:** 10.1016/j.apsusc.2005.07.123
16. Dupas-Bruzek, C.; Robbe, O., Addad, A.; Turrell, S.; Derozier, D.; *Appl. Surf. Sci.,***2009**, *255*, 8715-8721. **DOI:** 10.1016/j.apsusc.2009.06.025
17. Zundahl, S.S. ; Zumdahl, S.A. ; Chemistry. 8th ed. Brooks/Cole, CENGAGE Learning, Belmont, CA 94002-3098 USA 2010, Table 8.4 on p. 362. ISBN-13: 978-0547168173 ISBN-10: 0547168179
18. Kelly, M.A., Analysing insulators with XPS and AES. In: Briggs D, Grant JT, editors. Surface Analysis by Auger and X-ray Photoelectron Spectroscopy, IM Publications, Chichester, UK, **2003**. pp. 191-210.
19. Hofmann, S., Auger- and X-ray Photoelectron Spectroscopy in Materials Science. A User-Oriented Guide, Springer-Verlag, Berlin, Heidelberg, **2013**.
20. Beamson, G; Briggs, D., editors. The XPS of Polymers Database, Surface Spectra Ltd., Manchester, UK, 2012, ISBN 0-9537848-4-3.
21. Louette, P.; Bodino, F.; Pireaux, J-J.; *Surf. Sci. Spectra*, **2005,** *12*, 38-43. **DOI:** 10.1116/11.20050908
22. Alexander, M.R.; Short, R.D; Jones, F.R.; Michaeli, W.; Blomfield, C.J., *Appl. Surf. Sci.* **1999,***137,*179-183. **DOI:** 10.1016/S0169-4332(98)00479-6
23. O'Connor, J., Ion beam methods. In: Wandelt K, editor, Surface and Interface Science. Volume 1, Wiley VCH, Weinheim, Germany, **2012**, pp.269-310. ISBN: 978-3-527-41156-6
24. O'Hare, L-A.; Parbhoo, B.; Leadley, S.R.; *Surf. Interf. Anal.*, **2004**, *36*, 1427-1434 **DOI:** 10.1002/sia.1917
25. Wagner, C.D.; Riggs, W.M.; Davis, L.E.; Moulder, J.F.; Muilenberg, G.E.; editors. Handbook of X-Ray Photoelectron Spectroscopy, A Reference Book of Standard Data For Use In X-Ray Photoelectron Spectroscopy, Perkin-Elmer Corporation, Physical Electronics Division 6509 Flying Cloud Drive Eden Prairie, Minnesota, USA, **1979**.
26. Alam, A.U.; Howlader, M.M.R.; Deen, M.J.; *J. Solid State Sci. Technol.*, **2013**, *2*, P515-P523 **DOI:** 10.1149/2.007312jss
27. Holgerson, P.; Sutherland, D.S.; Kasemo, B.; Chakarov, D., *Appl. Phys. A*. **2005**, *81*, 51-56. **DOI:** 10.1007/s00339-004-3082-3
28. Griffith, G.W., *Ind. Eng. Chem. Prod. Res. Dev.,* **1984**, *23*, 590-593. **DOI:** 10.1021/i300016a015
29. Pitts, J.R.; Thomas, T.M.; Czanderna, A.W.; Passler, M.; *Appl. Surf. Sci.*, **1986**, *26*, 107-120. **DOI:** 10.1016/0169-4332(86)90056-5
30. Chao, S.S.; Takagi, Y.; Lucovsky, G.; Pai, P.; Custer, R.C.; Tyler, J.E.; Keem, J.E.; *Appl. Surf. Sci.*,1986; *26*, 575-583. **DOI:** 10.1016/0169-4332(86)90128-5
31. Finster, J.; Klinkenberg, E.-D.; Heeg, J.; *Vacuum*, **1990**, *41*,1586-1589 **DOI:** 10.1016/0042-207X(904)9025-L
32. Graubner, V.-M.; Jordan, R.; Nuyken, O.; *Macromolecules*, **2004**, *37*, 5936-5943. **DOI:** 10.1021/ma049747q
33. Donzel, C.; Geissler, M.; Bernard, A.; Wolf, H.; Michel, B.; Hilborn, J.; Delamarche, E.; *Adv. Mater.* **2001**, *13*, 1164-1167. http://dx.doi.org/10.1002/1521-4095(200108)13:15%3C1164::aid-adma1164%3E3.0.co;2-s
34. Ni, X.; Zhao, Q.; Zheng, H.; Li, B.; Song, J.; Zhang, D.; Zhang, X.; *Eur. J. Inorg. Chem.* **2005**, 4788–4793 **DOI:** 10.1002/ejic.200500453
35. Zhao, X.; Muench, F.; Schaefer, S.; Brötz, J.; Duerrschnabel, M.; Molina-Luna, L.; Kleebe, H.-J.; Liu, S.; Tan, J.; Ensinger W.; Electroless decoration of macroscale foam with nickel nano-spikes: A scalable route toward efficient catalyst electrodes, *Electrochem. Communic.*, **2016**, *65*, 39–43 **DOI:** 10.1016/j.elecom.2016.02.002
36. Wise, K.D.; Angell, J.B.; Starr, A.; *IEEE Trans. Bio-Medical Engin.* **1970**, *17(3)*, 238-247. https://www.ncbi.nlm.nih.gov/pubmed/5431636